FRINGE 96

Cross-Compatibility of ERS-SLC Products

A. Barmettler, P. Pasquali, D. Small and D. Nüesch

Remote Sensing Laboratories (RSL)
University of Zürich, Winterthurerstrasse 190, CH-8057 Zürich, Switzerland
barmettler@rsl.geo.unizh.ch
http://www.geo.unizh.ch/rsl/

Abstract

The SAR image products (ERS-SLC) from the ERS AMI sensor are produced and distributed by various PAFs, such as CPRF, I-PAF and D-PAF. For high end applications that fully exploit the phase information of the coherent recording system (i.e. interferometric applications / DEM generation) the feasibility of combining products from different processing facilities is important. During this study, the level of cross-compatibility of SLCs was assessed by comparing interferograms and coherence maps which exploit combinations of pairs of SLCs. This included auto-interferograms from different processors. The conclusions is that the tested SLC products can be exchanged without a significant increase of the phase noise. Nevertheless, high precision measurements must take into account the systematic errors - phase offset and trend - introduced into the data.

Keywords *- SAR-Interferometry, Phase Noise, Image Quality, SLC, PAF*

Introduction

The user community has an interest in performing SAR Interferometry by using existing SLC (Single Look Complex) images, without having to take into account which PAF (Processing and Archiving Facility) produced them. The requirements for SLC images are described in the *ERS.SAR.SLC-I Product Specifications* (ESA Pub., 1995), where a number of tests are defined, e.g. to confirm the phase preservation during the processing. However, these tests do not ensure the cross-compatibility of the images processed by different SAR processors for high quality SAR interferometry, since they check mainly the quality of the azimuth compression algorithm rather than the overall performance of the processor.

The interferometric phase depends heavily on the surface structure. To be representative of as many applications as possible, the chosen test scenes included areas with a large variety of coherences. We used two different tandem scenes, acquired over Bern (Switzerland) and Cairo (Egypt), respectively. The Bern tandem data from 13/14 August 1995 covers agricultural, forest and urban areas as well as lakes: a mid to low level of coherence was observed in this area.

The Cairo scene comprises larger regions with rocks and dry areas to provide a completely different coherence distribution. The desert area south-west of Cairo showed high temporal coherence on the tandem 1-day repeat data from 19/20 November 1995.

The SLC images received from SAR processors used at CPRF (Central Processing Reference Facility, ESRIN) - ESA VMP (Verification Mode Processor) - and I-PAF (ASI) were analysed and their CEOS parameters and Doppler spectra compared. This was important for the interpretation of the interferograms and its statistics, which were processed subsequently from each pair of the SLC products. The InSAR processing was performed using our in-house developed interferometric SAR processor ISP and Zürich InSAR Processor (ZIP).

Doppler Centroid

The azimuth spectrum contains information about the Doppler shift, and its bandwidth is related to the spatial resolution in the azimuth direction. For the interpretation of the coherence map statistics the knowledge of the relative resolution between the SLC images is required.

Figure 1 presents the averaged total azimuth power spectra for the Cairo SLC. It is evident that ERS-1 and ERS-2 spectra have their maxima at a different Doppler frequency (i.e. the Doppler centroid frequency) due to different squint angles. In interferometric processing, one has to avoid relating the not common spectral parts by filtering. However, the systems have the same spectral shape and the same processed and even a corresponding half-power bandwidth of about 605 Hz (both, Cairo and Bern, 36% of the PRF of 1679.9 Hz). On the other hand, the values indicated for the processed Doppler bandwidth in the CEOS header differ significantly, probably using different definitions of the term "bandwidth".

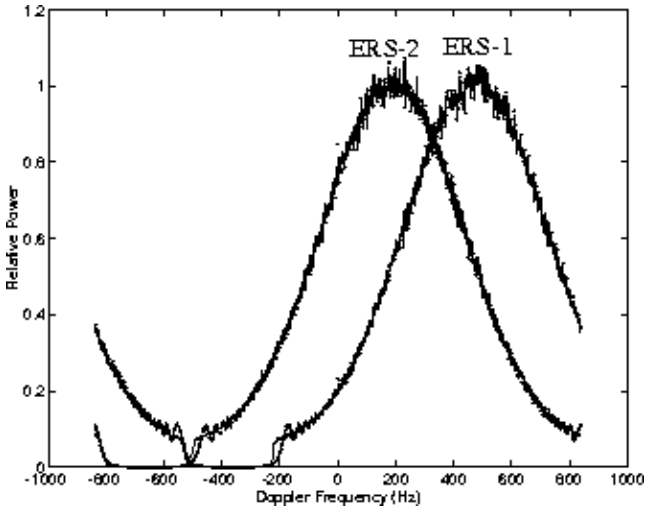

Figure 1: Relative azimuth power spectrum of ERS-1 (right) and ERS-2 for CPRF (solid line) and I-PAF (dot ted). Bern test site.

The Doppler centroid frequency (the frequency of the spectra's maximum) is a main driver for accurate azimuth focusing. Since it depends on the Earth's rotation and satellite yaw steering, it varies in slant range. This dependency is usually approximated by a polynomial of small degree. In Figure 2 the polynomials given in the header files are plotted and compared with the calculated average of the Doppler Centroid frequency for the ERS-2 SLC processed by RSL. All PAFs use polynomials of small degree to represent the range dependency of the Doppler Centroid frequency. The CEOS third order polynomials used by the CPRF and D-PAF show inconsistencies compared to our own estimation from raw data, whereas I-PAF represents an acceptable linear fit.

The Centroid shows a high dependence on the mean altitude above sea level. For ERS the azimuthal displacement is in the order of 100 m per 1000 m change in altitude, which corresponds to -30 Hz. Therefore it is important to use an algorithm that takes as many azimuth samples as possible into account to mitigate this topographic influence. If this is not the case, the Doppler Centroid is expected to show a significant dependence on azimuth position, and thus shows a high variability compared to the mean value of the Doppler Centroid over the whole scene.

If one estimates the Doppler Centroid by exploiting the final SLC product one finds a good representation of the polynomial used during focusing, as expected since the Doppler Centroid is projected into the data.

However, the polynomials used at CPRF and D-PAF show significantly different coefficients and the I-PAF even a different polynomial degree, hence the parameters or the software to estimate the Doppler centroid frequency must be different among these PAFs.

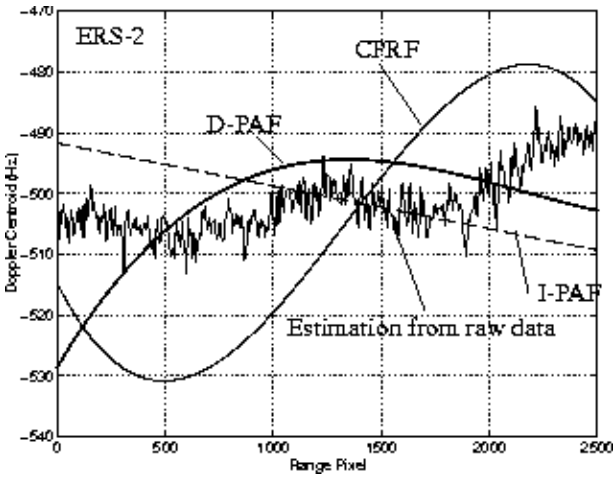

Figure 2: Doppler Centroid variation along slant range for ERS-2 from Cairo processed at the various PAFs. The polynomial coefficients are taken from the SLC CEOS leader files. Estimation is the 10 point average with an FFT size of 8192 samples.

Interferograms

More than a dozen interferograms were computed and analysed. To distinguish auto-interferograms and tandem interferograms, the terms *Singletrack* and *Multitrack* are introduced. *Singletrack* means that the identical original raw data from the sensor is processed at different PAFs and that these products are compared. *Multitrack* is the common tandem configuration of ERS-1 and ERS-2. ERS-1 is considered the master track within this report.

Singletrack

Singletrack interferograms provide a useful way to compare the SAR processors. To calculate the phase difference of the two images, a coregistration had to be performed. This resulted in a shift in range of none to several pixels, whereas the azimuth offset additionally showed a subpixel offset. The observed range offset must be explained by inaccurate time-referencing of the SAR processors. The azimuth shift of up to thousands of pixels is originated by the non-standardized starting time of the frames and differences in the sensor velocities used for focusing, together with inaccurate azimuth time-referencing.

The phase statistics of the coregistered auto-interferograms are compiled in Table 1. The value of the interferometric phase between SLC from the various PAF was almost constant but non-zero. According to the requirement of Phase Preservation of the SLC (ESA Pub., 1995), the zero phase of the azimuth filters are designated to the zero Doppler point in the time domain. Since the auto-interferograms act similar to the interferometric offset processing test proposed in (ESA Pub., 1995), we expected a mean phase of less than 0.1 degrees. The observed phase bias leads to the assumption that at least one of the tested SAR processors has problems with phase preservation. Most likely this is due to differences in the Doppler centroid estimation.

Cairo	Interferogram	Mean Phase Value (deg)	Std Dev Phase (deg)
ERS-1	CPRF / I-PAF	306.5	3.50
ERS-1	CPRF / D-PAF	189.1	3.04
ERS-2	CPRF / I-PAF	155.8	2.98
ERS-2	CPRF / D-PAF	10.3	3.21

Table 1: Singletrack interferogram of SLC products. Cairo site.

This observed variability of the mean interferometric phase implies that absolute phase measurement (besides the 2π ambiguity) is still not possible. However, each processor passes the requirement on the standard deviation of the interferometric phase. It lies below the limit of 5 degrees.

It was a surprise to observe that the CPRF and D-PAF processors do not show a smaller standard deviation, since both are assumed to use identical source code. Though, if the start time in azimuth is different between CPRF and D-PAF, the final products are not identical, and could show the observed variation on the same level as two different processors do. Therefore it is still possible that the processors have the same source code.

This random phase offset could be a problem when mosaicing full frame or quarter scene images: the phase continuity at the border would not be guaranteed.

In the following we tested for a systematic error in the phase, i.e. a dependency on range or azimuth position. Figure 3 reveals no phase trend in azimuth for the auto-interferograms. Moreover, the mean phase stays in the interval of 0.1 degrees.

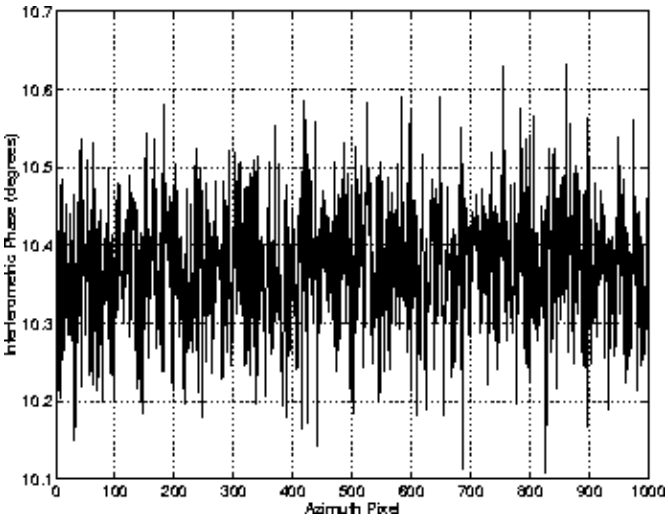

Figure 3: Interferometric phase variation along azimuth direction for the CPRF / D-PAF interferogram. ERS-2, Cairo area.

On the other hand, Figure 4 reveals a systematic phase trend in the range direction on the order of 0.6 degrees. This phase trend in range is most probably due to differences in the polynomial used to approximate the Doppler Centroid frequency as a function of range, and hence the Doppler Centroid estimation software.

We believe that it is less important that the Doppler Centroid estimation is a perfect representation of the physical Doppler Centroid frequency than that the various PAFs calculate the data using the same algorithm and polynomial order.

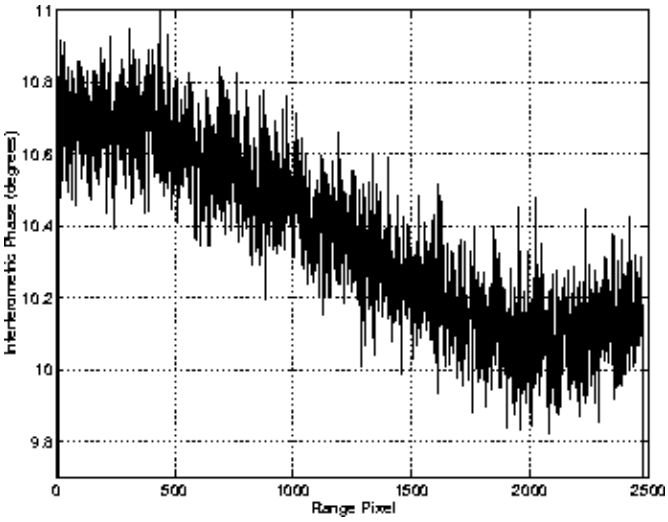

Figure 4: Interferometric phase variation along range direction for the CPRF / D-PAF interferogram. ERS-2, Cairo area.

Multitrack

The generation of the multitrack interferogram is the conventional task of producing a tandem interferogram. Figure 5 and 6 show the 2π fringes of the flattened interferogram. The resulting phase fringes have a periodicity equivalent to a change in height of about 150 m for the Bern interferogram and of about 40 m for Cairo.

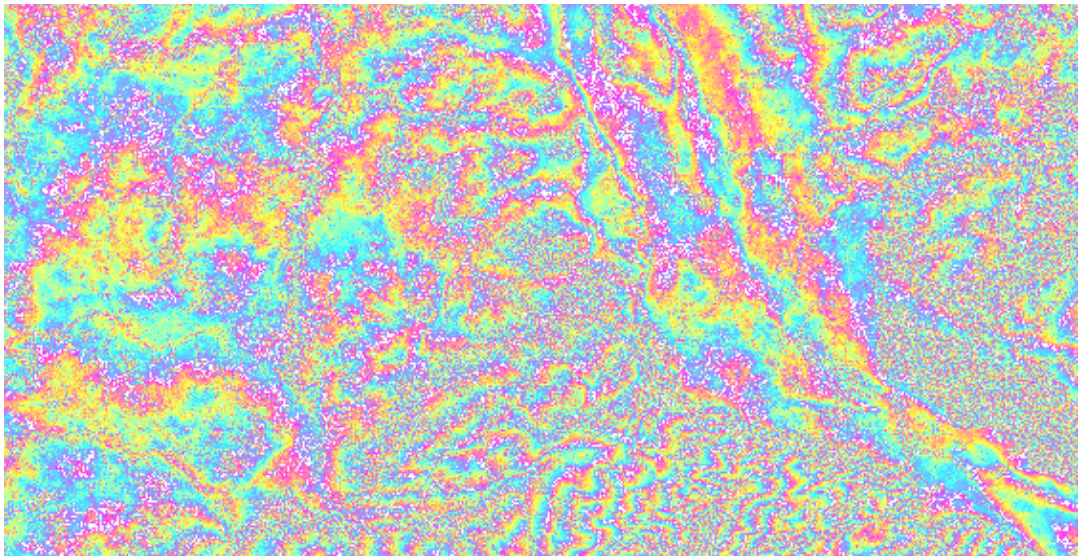

Figure 5: Flattened interferometric phase of ERS-1/ERS-2 for Bern. CPRF processing was used for both SLC.

The two interferograms confirm the choice of the two test sites: on the one hand there is the accurate and high-resolution interferogram from the flat and dry area around Cairo, which could be used for direct phase unwrapping without any further processing steps;

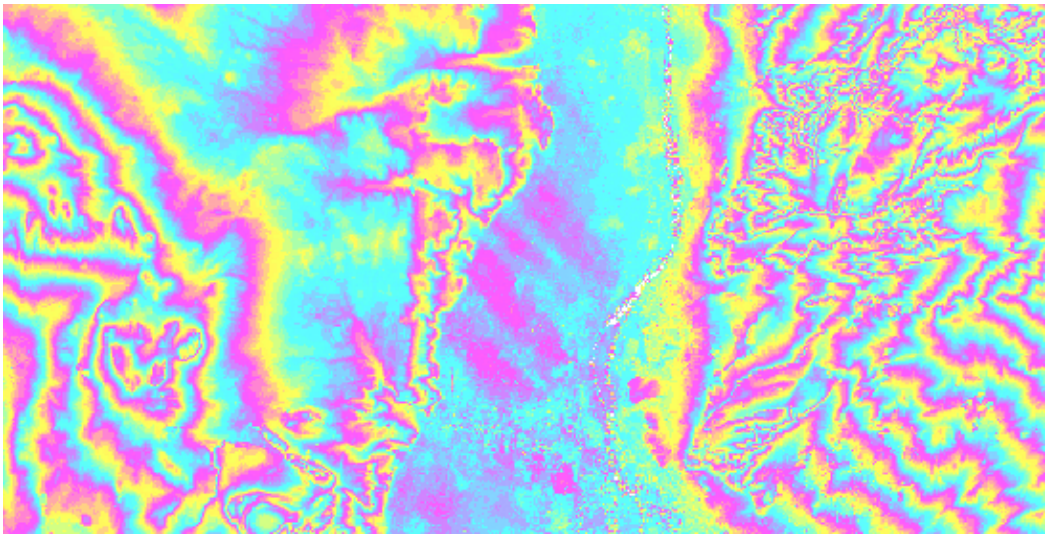

Figure 6: Flattened interferometric phase of ERS-1/ERS-2 for Cairo. CPRF. processing was used for both SLC.

on the other hand, the Bern interferogram appears noisy even in the one-day repeat tandem configuration and the rather short baseline. The production of a DEM would require numerous user interactions during the unwrapping task.

Coherence Maps

The coherence histograms and statistics are an indicator for the quality of the various processors. The processing of image pairs from the same raw data in particular reveals the relative phase differences introduced by the different processors.

Singletrack

Figure 7 shows the coherence that can be achieved when combining products from different SAR processors in the singletrack case. Notice how a difference, even if small, is present in the phase information provided by different focusing programs starting from the same raw data. The level of phase noise is directly related to the correlation coefficient (Bamler R. and Just D., 1993): the results presented in Figure 7 concerning the coherence distribution confirm the results seen in Table 1 in terms of phase noise.

In this case no systematic phase trends need to be considered as a source of coherence loss, since the estimation of the correlation coefficient is performed on relatively small subwindows. No temporal decorrelation effects are present in this combination: only image misregistration, differential defocusing and different processor noise levels are possible sources for this small loss of coherence.

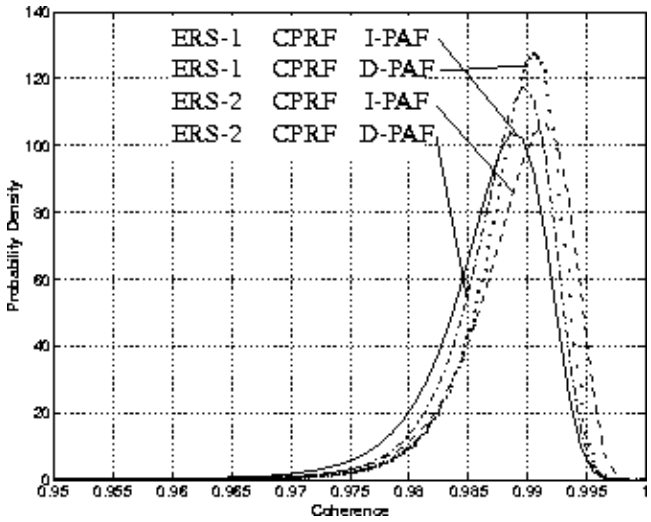

Figure 7: Coherence for Cairo images: solid ERS-1 CPRF / I-PAF; dotted ERS1 CPRF / D-PAF; dashed ERS-2 CPRF / I-PAF; dashdot ERS-2 CPRF / D-PAF.

Multitrack

The multitrack tandem coherence maps are also affected by the temporal decorrelation. The histograms in Figure 10 and 11 confirm again the choice of two completely different sites, by showing distinct distribution and maxima values.

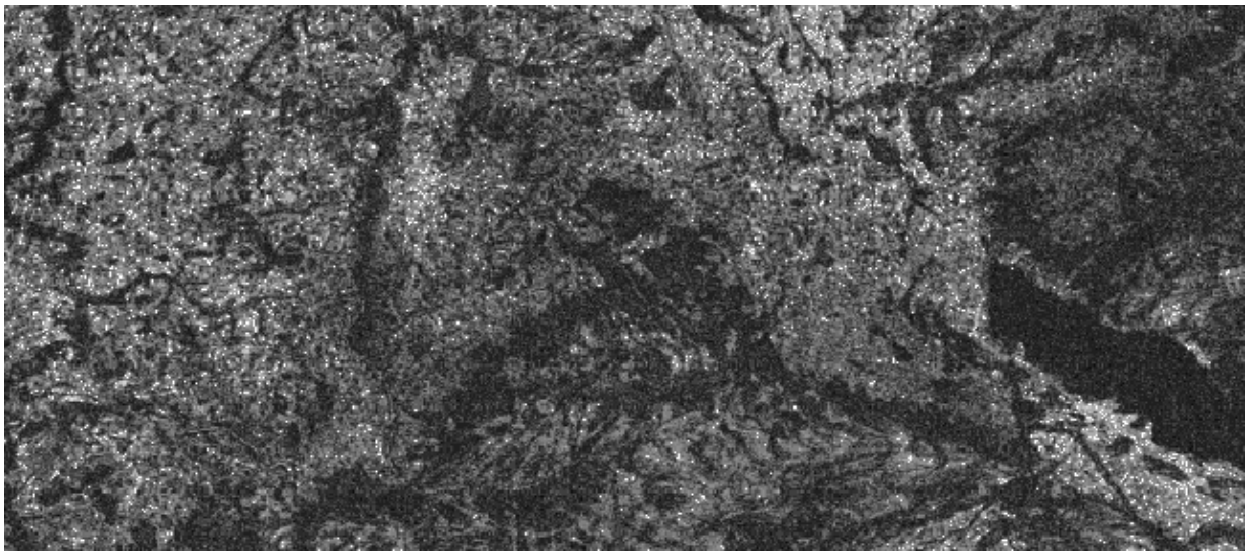

Figure 8: Coherence map of the Bern test site. SLCs processed at CPRF. White represents high coherence areas.

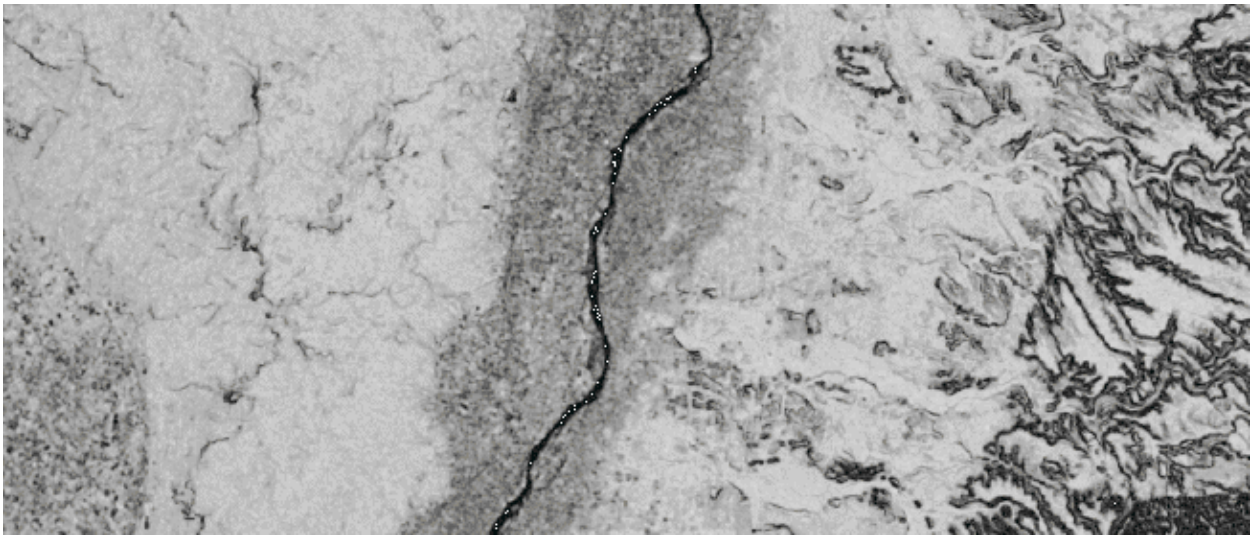

Figure 9: Coherence map of the Cairo test site. SLCs processed at CPRF. White represents high coherence areas.

For the Bern site (Figure 10), all calculated interferograms show about the same probability distribution function. Very small differences in the estimated coherence values are noticeable only when analysing the numerical results. No reasons appear from this test to suggest that one must necessarily use SLC pairs focused by the same processor to produce interferometric images.

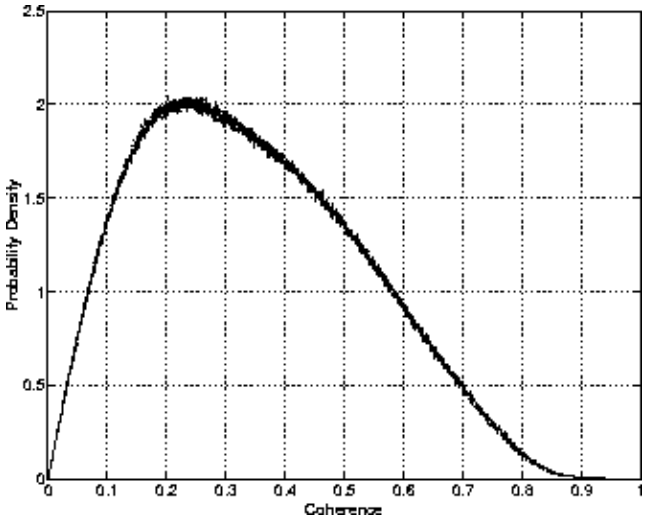

Figure 10: Coherence for ERS-1/ERS-2 Tandem images over Bern. Following combinations are used; I-PAF/CPRF, I-PAF/I-PAF, CPRF/CPRF, CPRF/I-PAF.

For the Cairo site (Figure 9) some differences can be noticed between the different coherence maps obtained from the various SLC combinations. Table 2 compiles the figures of statistics. The mean coherence of an interferogram produced using SLCs from different processors is not necessarily lower than that obtained from SLC produced by the same processor: on the contrary, the maximum value of coherence for this site was obtained by exploiting two data sets focused by different processors.

Cairo		Mean Coherence	Std Dev of Coherence
ERS-1	ERS-2		
CPRF	CPRF	0.6961	0.1526
CPRF	I-PAF	0.7025	0.1549
I-PAF	CPRF	0.6599	0.1445
I-PAF	I-PAF	0.6757	0.1476

Table 2: Coherence statistics for the tandem interferograms. Cairo site.

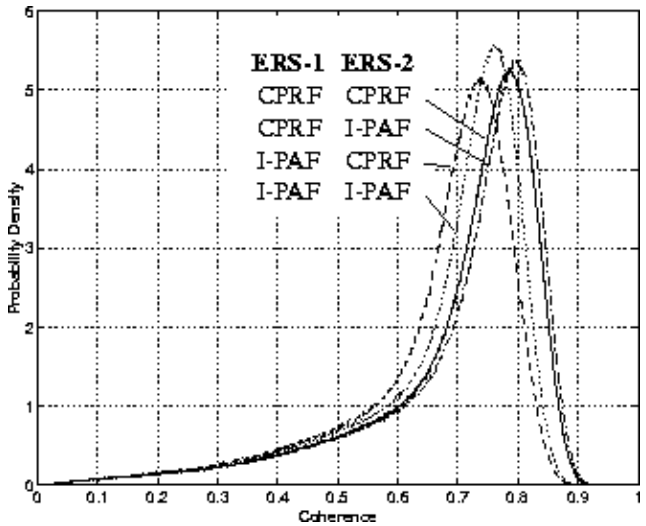

Figure 11: The coherence for ERS-1/ERS-2 Tandem images over Cairo. Starting from left: I-PAF/C-PAF (dashed), I-PAF/I-PAF (dotted), CPRF/CPRF (solid), CPRF/I-PAF (dash-dotted).

The observed coherence differences can be explained in terms of residual defocusing effects (Monti Guarnieri A., 1996), differences in the focusing algorithms and considering the normal variability of the phase noise introduced by every processor.

Conclusions

Although this study revealed some remarkable qualitative results, we could not perform further tests to get better statistics for quantitative data extraction. It should be kept in mind that only a small data set has been used within this analysis.

The investigated SLC image did not show any anomalies, i.e. sidelobe artefacts or saturated areas. However, the tested processors are not compatible with respect to the Doppler Centroid estimation. The values for this frequency deviates by as much as 50 Hz compared at one specific range distance. The Doppler Centroid frequency dependency on range is represented by polynomials of a degree not consistent among all PAFs. This uncertainty may be the source for a random phase offset introduced into the SLCs. In turn, this may lead to a phase inconsistency when stepping quarter scenes to full frames (or full frame images to larger mosaics), and makes reconstruction of the absolute phase of the interferometric products without the use of ground control points impossible.

Auto- and differential interferograms showed a phase trend in the range direction over a quarter scene swath, whereas the mean interferometric phase in the azimuth direction was observed to be constant. This phase trend is probably introduced by the SAR processors and leads to systematic errors in the reconstructed DEMs. The influence of this trend is larger in interferometric applications with small baselines.

The product specifications (ESA Pub., 1995) point out that SLC-I products consist of a full frame. To date, most of the operational SAR processors (suitable for SAR interferometry) have only been capable of processing single quarter scenes at a time. Thus, for larger-scale interferometry, a full scene is assembled from four independently processed parts, with the possibility of introducing a phase inconsistency at the borders. Hence, the phase trends and discontinuity will become more severe when considering full frames.

Most important, the InSAR processing of SLC data from different PAFs did not increase phase noise. The user can combine SLCs from various PAFs for producing interferograms without a loss of the overall quality.

However, there are some secondary restrictions to the cross-compatibility: e.g. areas covered by the SLC are not standardized, especially the azimuth times. This may lead to a shift of up to 25% of the length of corresponding quarter scenes. The parameters included within the CEOS header are defined differently for each PAF (i.e. I-PAF and CPRF even indicate different wavelengths, pulse repetition frequencies, and spatial resolutions). Some of these data seem to be in disagreement with the image positions. ESA has announced its intention to harmonize the time-referencing of the processors and CEOS header format used at ESA PAFs.

Acknowledgement

This work emerged from an ESA contract study addressed to ESRIN, Rome. We like to thank ESA for the generous provision of the required ERS images.

References

Bamler R. and Just D., 1993
Phase Statistics and Decorrelation in SAR Interferograms, Proc. IGARSS `93, pp. 980-984.

Barmettler A., *et. al.*, 1996
Cross-Compatibility of ERS-SLC-I Products, Report to the ESA/ESRIN, RSL Zürich.

Cattabeni M., *et. al.*, 1994
Estimation and Improvement of Coherence in SAR Interferometry, Proc. IGARSS '94, pp. 720-722.

ESA Pub., 1995
ERS.SAR.SLC-I Product Specifications, ESA Doc., Issue 1.

Goodman N.R., 1963
Statistical Analysis Based on a Certain Multivariate Complex Gaussian Distribution, Ann. Math. Statist., Vol. 34, No. 152, pp. 152-180.

Monti Guarnieri A., 1996

Residual SAR Focusing: An Application to Coherence Improvement, in IEEE Trans. GRS, Vol. 34, No. 1, pp. 201-211.